Synthesis and Caracterization of Mesoporous FePO4 as Positive Electrode Materials for Lithium Batteries

Amel Salamani[a, *], Abdallah Merrouche[a, **], Laid Telli[a, *], Pedro Gómez-Romero[b], and Zahilia Caban Huertas[b]**

[a]*Laboratoire des Matériaux Inorganiques, Université Mohamed Boudiaf—M'sila, 28000 Algeria*

[b]*Centre d'Investigació en Nanociència i Nanotecnologia, CIN2 (CSIC-ICN), Campus UAB, Bellaterra, Barcelona, E-08193 Spain*

*****e-mail: amelslam@yahoo.fr*

******e-mail: abmerrouche@yahoo.fr*

*******e-mail: laidtelli@yahoo.fr*

Abstract— Mesoporous iron phosphates were synthesized using sodium dodecyl sulfate (SDS) and cetyltrimethylammonium bromide (CTAB) as surfactants. The material synthesized in the presence of SDS was not applied as a positive electrode active material of a lithium battery. The results show that the obtained FePO4 has a mesoporous structure with a specific surface area of 70 m2 g^{-1} and a dominant pore diameter of 3 nm. Those mesoporous were characterized by different microstructural and electrochemical analyzes. Among the materials studied under different conditions, those calcined at 450°C preserve mesoporous structures and exhibit the best electrochemical performance when used as active materials of the positive electrodes of lithium batteries. Effectively, a relatively high specific capacity of 135 and 122 mAh g^{-1} was registered at C/20 collected experimentally by the samples synthesized in the presence of SDS and CTAB, respectively.

***Keywords*:** lithium batteries, positive electrodes, mesoporous materials, iron phosphate, electrochemical tests

INTRODUCTION

The iron-based cathode materials, such as $FePO_4$ and $LiFePO_4$, are attractive for usage in lithium batteries because they are low-cost and environmentally friendly and have a high theoretical capacity [1–8]. For instance, $FePO_4$ has a theoretical capacity of 178 mAh g^{-1} per 1 mol of the lithium intercalated and a discharge voltage from 3.5 to 2.5 V [1]. However, the behavior of these materials has two disadvantages: a slow diffusion of Li^+ in the structure and a very low electronic conductivity. Therefore, the combination of a porous structure and an electronic conductor (carbon) can overcome these drawbacks.

Recently, $FePO_4$ mesoporous materials with a large specific surface have found many applications, including in lithium batteries [9–15]. However, few synthesis methods of getting mesoporous $FePO_4$ with a large specific surface, using surfactants, are indicated [16–18]. A mesoporous $FePO_4$ was synthesized as cathode material using CTAB as templating agentand the compatibility of this compound with other components of lithium cells was demonstrated [15]. A surfactant (EO_{20}–PO_{70}–EO_{20}, Pluronic P123) was used to show the role of the mesoporous structure in improving the kinetics of intercalation of lithium ions in the host material [17]. Later, other authors [19, 20] were able to increase the specific surface area of these materials by improving the synthetic process, which engendered in a better electroactivity. In addition, using SDS as surface active agent made it possible to prepare mesoporous $FePO_4$ with a large surface area [16]. However, these materials have not been characterized electrochemically.

In this work, we aimed at synthesizing mesoporous $FePO_4$, using SDS as structuring agent, and at demonstrating its use as an active material for the positive electrode in lithium batteries. A comparison of the electrochemical performance of this material with that of a material synthesized in the presence of CTAB and the effect of the heat treatment was a part of our objective.

EXPERIMENTAL

Synthesis

The synthesis of a mesoporous structure was based on the procedure described in [1] The article is published in the original. [16]. To this end, 8.08 g of $Fe(NO_3)_3$ (99%) and 7.16 g of Na_2HPO_4 (99%) were dissolved

separately in 80 g of distilled water; the two solutions were then stirred and mixed. The resulting precipitate ($FePO_4$) was recovered by centrifugation and washed with distilled water, then dispersed in 20 g of distilled water. Finally, 1.32 g of HF (40%) was added under rigorous agitation. After obtaining a clear solution, 2.88 g of SDS (99%) was dissolved in 10 g of distilled water and then added to the above solution with stirring; the mixture was agitated for 30 min at room temperature and then transferred to an oven at 60□C for 2.5 h. After cooling to room temperature, a light yellow precipitate was collected by centrifugation and washed several times with water and acetone. The collected solid was dried at room temperature. The as synthesized product (denoted SDS-B) was the base of the first series of our samples.

The second series of samples was prepared by the same previous procedure, but using CTAB instead of SDS as the surfactant [15]. After the step of cooling at ambient temperature, no precipitate was observed.Thereby, increasing the pH solution from 2 to 10 byadding 1 M of tetraethylammonium solution yields ayellow precipitate that was collected by centrifugation and washed several times with distilled water and acetone and then allowed to air dry (denoted CTAB-B).

In order to extract surfactants, SDS-B and CTAB-B have been submitted to ion exchange according to the protocol proposed in [21]. Typically, 0.7 g of eachsample is mixed with 50 ml of a 0.05 M ethanol solution of sodium acetate, with stirring for 40 min at room temperature. The solids recovered by centrifugation have been washed to ethanol and dried at room temperature: they are denoted SDS-E and CTAB-E, respectively. Furthermore, to evaluate the effect of calcination on the electrochemical performance of these materials, the synthesized samples have been also submitted to a thermal treatment for 4 h under argon at 450 (denoted SDS-B-450 and CTAB-B-450)and 600□C (denoted SDS-B-600 and CTAB-B-600).

Characterization

X-ray diffraction (XRD) patterns were recorded on a Rigaku D-Max-Ultima III diffractometer, using Cu*K*□□radiation (□□= 1.5406 A). The data were collected in the 2□□range between 0.6□□and 10□□in step of 0.02□. The nitrogen adsorption and desorption isotherms were measured at 77 K using a QUANTACHROME NOVA 2000 apparatus. The specific surface area was calculated by the Brunauer–Emmett– Teller (BET) analysis method and the pore size distribution was calculated by the

method of Barrett– Joyner–Halenda (BJH). The microstructural and morphological characteristics of the iron phosphate powders were examined with a transmission electron microscope (TEM) JEOL JEM 1230. The analysis by the Fourier transform infrared spectroscopy (FTIR) was carried out with a Shimadzu spectrometer 8400S, used in the transmission mode. The spectra were recorded in the interval 4000–400 cm^{-1} on KBr based pellets with a resolution of 4 cm^{-1}.

Cell Fabrication and Testing

The electrochemical measurements (cyclic voltammetry and chronopotentiometry) were performed on lithium cells with two electrodes. These cells were subjects to the following electrochemical chain: lithium metal/liquid electrolyte ($LiPF_6$: 1 M) in a mixture of ethylene carbonate: dimethyl carbonate (1 : 1)/positive electrode. The electrode was composed of an active material (85 wt %) and carbon black (10 wt %), to improve the electronic conductivity of the electrode, and polyvinylidene fluoride solid (5 wt %) as binder. The whole was dispersed in a solvent of 1-methyl-2-pyrrolidinone (Sigma-Aldrich, 99%) and stirred for5 h. The suspension was applied onto an aluminium current collector and, after drying under vacuum at80□C for 12 h, the working electrodes were cut and weighed for electrochemical testing. The lithium metal was used as negative electrode and also as reference electrode. A CelgardR 3501 membrane soaked in the electrolyte separated the electrodes in order to avoid possible internal short circuits. Electrochemical cells were treated in pieces of the SwagelockR type in a glove box under argon atmosphere and electrochemical study was realized by using a potentiostat EC-Lab(BioLogic).

RESULTS AND DISCUSSION

Physicochemical Characterization

The XRD patterns of mesoporous materials are very special because they have few peaks relatively wide and located at the small angle. Figures 1 and 2 show the diffractograms obtained.

A single diffraction peak at 2θ=1.2º is clearly observed on the diffractogram of the SDS-B sample (Fig. 1, line *a*), characteristic of a mesoporous iron phosphate [15, 16, 22, 23] with a disordered arrangement of the channels [8, 24]. However, the diffractogram of the SDS-E sample shows two reflections at 1.18 and 1.48 (Fig. 1, line *b*), and that of SDS-B-450— at 0.9º and 1.5º (Fig. 1, line *c*).

This confirms the fact that the mesoporous structure is preserved after the elimination of the surfactant or calcination at 450 C. The appearance of a second peak may be explained by a better pore organization due to the surfactant removal by chemically or thermally [8].

The XRD patterns at small angles of the samples synthesized using CTAB (CTAB-B, CTAB-E and CTAB-B-450) are shown in Fig. 2, with three diffractograms exhibiting similar behavior of the samples. In the diffraction patterns, only one peak around 0.8º is present. This is in good agreement with the results in the diffractograms of the mesophases of CTAB-E and CTAB-B-450 indicates that they are less ordered than those of SDE-E and SDS-B-450 [15].

The nitrogen adsorption–desorption isotherms are shown in Figs. 3 and 4, exhibiting a typical shape of a mesoporous material, which is in agreement with literature [25–27]. Indeed, a saturation bearing develops at a high relative pressure and this saturation corresponds to the activities of mesoporous materials. Furthermore, a clear hysteresis is observed between the adsorption and desorption curves corresponding to an irreversible adsorption–desorption phenomenon. According to the IUPAC classification, the obtained isotherms are typical type IV isotherms. In the case of SDS-E (Fig. 3) and CTAB-E (Fig. 4), the hysteresis loop appears at the relative pressure P/P_0 higher than 0.8. This is due to the swelling of the sample during the adsorption (swelling intergranular); a similar effect has been already observed for different mesoporous materials: among them MCM-41 mesoporous silica[28, 29].

The isotherms related to SDS-B-450 and CTABB-450 samples calcined at 450ºC under argon are also of type IV, with a lower closure point of the hysteresis at $P/P_0 \approx 0.4$. The same phenomenon has been reported in literature [7, 8, 30, 31]. However, for as the synthesized samples of SDS-B and CTAB-B, the mesoporosity does not seem to be accessible duringadsorption. This is presumably due to the occupation of the pores by surfactants.

The pore size distribution curves (insets of Figs. 3and 4) show that the samples eliminated the pores with diameters in a range of 1.5 and 4.0 nm, which is conventional with the pore size of mesoporous $FePO_4$ [20, 32]. The pore size distribution curve is heterogeneous, with a broad peak centered at 3.0 nm. The obtained nano-$FePO_4$ has a mesoporous structure with the intra-particle porosity rather than the inter-particle one [20, 32]. However, micropores of a large size can be observed beside mesopores

whose diameter is about 1.0 nm. Similar results have been reported elsewhere [32]. The insets of Figs. 3 and 4 show that the pores diameters for SDS-B-450 and CTAB-B-450 samples are getting smaller. This is probably due to the contraction of the mesoporous structure [8, 17, 31]and the formation of the residual carbon in the pores[19]. These results are supported by those evidenced by isotherms and the XRD data.

The physical characteristics deducted from the nitrogen adsorption–desorption isotherms of the samples synthesized (Table 1) show that among the studied samples, SDS-E and CTAB-E have the most important porous volumes and pores with diameters due to the removed of the organic matter. However, the calcination of as synthesized samples at 450 °C generates an enlargement of the specific surface area and a decrease of the total volume and of the average diameters of mesopores. This can be explained by the fact that the existing surfactant, in the pores and between the particles, can be transformed into porous carbon after the heat treatment [19]. Moreover, the samples prepared in the presence of CTAB show specific surface areas and pore volumes higher than those of the samples obtained using SDS, which may be due to the lengths of the chains of two surfactants.

Figure 5 shows TEM images of the SDS-E, SDSB-450, CTAB-E and CTAB-B-450 samples. The mesostructured can be observed in all samples. These images reveal that the samples in Figs. 5a, 5c possess nanometric particles, slightly agglomerated; each agglomeration is constituted of several primary particles, thereby the mesostructure is entirely similar to that found in a mesoporous iron phosphate [8, 17, 19, 20].

The images in Figs. 5b, 5d allow confirming that particles of small sizes (some tens of nm) are assembled to form porous aggregates. However, the heat treatment engenders modifications in the mesostructured and a significant reduction in the size of the interparticle pores. This is likely due to the pyrolysis of structuring on the $FePO_4$ particle surface.

In order to confirm the result of elimination of surfactant pores of the mesoporous structure, we applied the FTIR spectroscopy to the as synthesized $FePO_4$ and to that which sustained the eliminating of structuring via chemical or thermal treatment (Fig. 6). The infrared spectra obtained are practically similar to that of iron phosphate [15, 17, 19, 33]. The FTIR spectra relating at the removed (SDS-E and CTAB-E) and as synthesized (SDS-B and CTAB-B) samples show a broad absorption band

around 3400 cm^{-1} and a peak of a strong absorption intensity centered at 1640 cm^{-1}, attributable to the O–H bond of the composition water. Moreover, a broad maximum around 1050 cm^{-1} that can be related to the P–O ibrations of polyanion was observed [33].

In Fig. 6a (spectrum *b*), absorption bands characteristics at about 2930, 2854, 1473 and 1250 cm^{-1} were observed. While on the spectrum *a* of the removed sample, these bands disappeared. This result confirmed the total elimination of the SDS surfactant.

Figure 6b shows the infrared spectra of the CTAB-E, CTAB-B and CTAB-B-450 samples. The existence of the bands at 2928 and 2847 cm^{-1} indicates that the surfactant is present as micelles in the mesostructured iron phosphate [15]. Thus, the bands at 1465 and 1388 cm^{-1} are attributed to the deformation of $–CH_2–$ and $–CH_3$ of the incorporated surfactants (spectrum (b)) [34].However, the peaks corresponding to the CTAB sample do not appear on the spectrum *a* of the sample removed via ion exchange.

After calcination at 450ºC, several bands of low intensities are observed in the regions 500–650 cm^{-1} and 900–1200 cm^{-1}, which can be attributed to the O–P–O asymmetric vibrations of the polyanion (spectra c) [17–19]. Moreover, a band attributable to the O–P–O symmetric vibrations is observed at 432 cm^{-1}. On the other hand, a band at 1030 cm^{-1} characteristic to Fe–O–P can be observed, which can serve to identify crystalline $FePO_4$ [19]. These FTIR spectra show that the characteristic peaks of the surfactant as well as those of the OH group have disappeared. These results prove the elimination of surfactant by both processes used.

Electrochemical Properties of the Synthesized Materials

The electrochemical behavior of the $FePO_4$ mesoporous materials synthesized with the SDS and CTAB as surfactant agents, used as positive electrodes for Li batteries, is investigated by cyclic voltammetry (CV), realized at room temperature into cells in two electrodes with lithium metal as negative electrode (Fig. 7). The reduction and oxidation peaks are well defined in the voltage range of 2.5 to 3.5 V, attributed to the Fe(III)/Fe(II) redox couple corresponding to the lithium insertion and extraction in the $FePO_4$ crystal structure [14, 17, 30, 35, 36]. This process appears to be reversible as shown in the voltammograms. These voltammograms, except that of the CTAB-B-600 sample, have a

single pair of reduction and oxidation peaks, indicating that there are no other electrochemically active species in the range of the potential chosen [30, 37]. The potential difference between the cathodic and anodic peaks is about 0.3 V comparable to that mentioned in literature [8, 38–43]. The voltammogram of CTAB-B-600 reveals that the redox reaction is effected in two successive steps. This indicates that the heat treatment at 600 °C engenders the formation of a closed second phase ($FePO_4$) or other species into impurity (Fe_xO_y) [8, 17, 20, 44].

Figure 7 indicates that the intensities of the cathodic and anodic peaks of the SDS-B and CTAB-B are lower. The ratio between the intensities of the peaks relative to the removed samples and those of the as synthesized samples are between 1.0 and 1.5. However, this ratio reached a value between 6 at 7 for SDSB- 450 and CTAB-B-450 samples. The experimental results of the CV indicate that among the studied samples $FePO_4$ calcined at 450 °C is the more electrochemically active versus the ion Li^+ ion insertion/ extraction.

Discharge tests were realized in the galvanostatic mode between 2.0 and 4.5 V vs. Li/Li^+ at C/20 regime. Initially, the batteries were tested in discharge, in order to try to intercalate lithium in the active material, following the reduction of Fe(III) to Fe(II).

Figure 8 shows the evolution of the cell voltage as function of the recovered discharge capacity and the lithium rate in Li_xFePO_4 ($0 < x < 1$) during the first discharge. The active material of the positive electrode for the cell is a mesoporous iron phosphate synthesized in the presence of SDS (Fig. 8a) or CTAB (Fig. 8b). The discharge curves (Fig. 8) have practically the same shape. In the first part, they present an abrupt voltage followed by a pseudoplateau of discharge when the average voltage of insertion of about 3 V vs. Li/Li^+, and then a lower less rapid decrease in the tension at the end of discharges. The discharge curves of the materials synthesized with SDS are shown in Fig. 8a. Figure 8a (line *c*) shows a voltage plateau clearly more expanded than in other materials with capacity, reported to the mass of $FePO_4$, of 135 mAh g^{-1}, corresponding to the lithium insertion around 0.78. The evolution of the lithium cell voltage using the samples synthesized with the CTAB as positive electrodes is shown in Fig. 8b. The discharge curve of the phase CTAB-B-450 presents the largest voltage plateau towards 3 V compared to that in other phases. Indeed, a capacity of 122 mAh g^{-1} was obtained during the first discharge, corresponding to the lithium insertion of about 0.70. This result is

comparable with that obtained using SDS. These electrochemical performances for SDS and CTAB are satisfactory and are similar to the best results reported for iron phosphate [15, 17].

In contrast, the capacity at the end of the first discharge does not exceed 25 mAh g^{-1} (13% of the theoretical capacity) for the as synthesized phases calcined at 600 °C. Also, the experimentally recovered capacity is approximately 10 mAh g^{-1} for the removed phases (5.2–5.8% of the theoretical capacity). Electrochemical cells using these samples as positive electrodes demonstrate very low electrochemical performance compared to that of the cells with the samples calcined at 450ºC.

The electrochemical study shows that the best performance of lithium batteries is produced with as synthesized materials calcined at 450ºC for both surfactants used. So, it appears that the optimum calcination temperature for this type of materials is around 450ºC. Indeed, the heat treatment at temperatures above 450ºC engenders lowering of the performance of the positive electrode generally attributed to the formation of a glassy surface phase [17, 20, 45, 46].

To provide more information about the electrochemical property of SDS-B-450 sample, cycling and rate capability were checked (Fig. 9). Figure 9a shows the discharge/charge curves at the first, 10th, 20th, 30th, 40th and 50th cycles; the material delivered a discharge capacity of 135.0, 134.5, 133.4, 132.3, 131.0 and 129.6 mAh g_{-1}, respectively, at C/20, exhibiting good cycling stability and high reversible capacity. In addition, the voltage difference between the charge and discharge pseudoplateaus did not increase significantly with increasing numbers of cycles, implying that the material possessed good electronic conductivity and high reaction reversibility. Figure 9b presents the cycling performance of the SDS-B-450 sample at C/20; the first discharge capacity is above 135.0 mAh g_{-1}. After 50 cycles, the capacity retention rate is 96%. It exhibits much better cycling stability. Figure 9c shows the discharge capacities of SDS-B-450 sample at C/20, C/10, C, 2C, 5C and 10C regime, which are 135.0, 129.0, 124.0, 113.7, 102.7 and 71.2 mAh g_{-1}, respectively. The discharge capacity decreases regularly under the increasing discharge rate, which is comparable to the previously reported $FePO_4$ cathodes [17, 33].

CONCLUSIONS

Mesoporous iron phosphates prepared using SDS and CTAB as surfactants were studied by various techniques. The results of XRD, TEM and nitrogen adsorption show that these iron phosphates have an ordered mesostructure with the dominant pore diameter between 1.0 and 4.0 nm and a specific surface area of about 70 $m_2\ g^{-1}$. The electrochemical study shows that the synthesized samples, obtained with SDS and CTAB and then calcined at 450□C, exhibit a remarkable electrochemical performance compared with that of the same type of materials used as active materials of the positive electrodes in lithium batteries. The maximal discharge capacity of 135 mAh g^{-1} is collected at C/20 regime and 129.6 mAh g_{-1} after 50 cycles. This exhibits a very good cycling performance.

ACKNOWLEDGMENTS

We would like to thank Professor Serge Kaliaguine and Dr. Bendaoud Nohair from the Department of Chemical Engineering, Laval University in Quebec, for their help in obtaining the nitrogen adsorption– desorption isotherms and their assistance in acquiring the TEM images. Professor Safia Hamoudi from the Department of Soil Sciences and Agri-Food Engineering, Laval University in Quebec, is also gratefully acknowledged for her assistance in acquiring the XRD patterns.

REFERENCES

1. Padhi, A.K., Nanjundaswamy, K.S., Masquelier, C., and Okada, S., *J. Electrochem. Soc*., 1997, vol. 144, pp. 1609–1613.

2. Padhi, A.K., Nanjundaswamy, K.S., and Goodenough, J.B., *J. Electrochem. Soc*., 1997, vol. 144, pp. 1188–1194.

3. Croce, F., D'Epifanio, A., Reale, P., and Settimi, L., *J. Electrochem. Soc*., 2003, vol. 150, pp. 576–581.

4. Song, Y., Yang, S., Zavalij, P.Y., and Whittingham, M.S.,*Mater. Res. Bull*., 2002, vol. 37, pp. 1249–1257.

5. Hong, Y.S., Ryu, K.S., Park, Y.J., Kin, M.G., et al.,*J. Mater. Chem*., 2002, vol. 12, pp. 1870–1874.

6. Shi, Z.C. and Yang, Y., *Prog. Chem*., 2005, vol. 17,pp. 604–613.

7. Lv, Y.J., Longa, Y.F., Su, J., Lv, X.Y., et al., *Electrochim.Acta*, 2014, vol. 119, pp. 155–163.

8. Trocoli, R., Morales, J., and Santos-Pena, J., *Solid State Ionics*, 2014, vol. 255, pp. 30–38.

9. Long, J.W., Dunn, B., Rolison, D.R., and White, H.S., *Chem. Rev*., 2004, vol. 104, pp. 4463–4492.

10. Shi, Z.C., Li, Y.X., Ye, W.L., and Yang, Y., *Electrochem.Solid State Lett*., 2005, vol. 8, pp. 396–399.

11. Liu, P., Lee, S.H., Tracy, C.E., Yan, Y.F., et al., *Adv.Mater*., 2002, vol. 14, pp. 27–30.

12. Kim, E., Son, D., Kim, T.C., Cho, J., et al., *Angew. Chem. Int. Ed*., 2004, vol. 43, pp. 5987–5990.

13. Kavan, L., Attia, A., Lenzmann, F., Elder, S.H., et al., *J. Electrochem. Soc*., 2000, vol. 147, pp. 2897–2902.

14. Prosini, P.P., Lisi, M., Scaccia, S., and Carewska, M.J., *J. Electrochem. Soc*., 2002, vol. 149, pp. 297–301.

15. Santos-Peňa, J., Soudan, P., Arean, C.O., and Palomino, G.T., *J. Solid State Electrochem*., 2006, vol. 10, pp. 1–9.

16. Guo, X., Ding, W., Wang, X., and Yan, Q., *Chem. Commun*., 2001, vol. 8, pp. 709–710.

17. Shi, Z.C., Attia, A., Ye, W.L., Wang, Q., et al., *Electrochim Acta*, 2008, vol. 53, pp. 2665–2673.

18. Mal, N.K., Bhaumik, A., Matsukata, M., and Fujiwara, M., *Ind. Eng. Chem. Res*., 2006, vol. 45, pp. 7748–7751.

19. Zhou, W., He, W., Zhang, X., Zhao, H., et al., *Mater. Chem. Phys*., 2009, vol. 116, pp. 319–322.

20. Qian, L., Xia, Y., Zhang, W., and Huang, H., *Microporous Mesoporous Mater*., 2012, vol. 152, pp. 128–133.

21. Holland, B.T., Isbester, P.K., and Balanford, C.F.,*J. Am. Chem. Soc*., 1997, vol. 119, pp. 6796–6803.

22. Yu, D., Wu, C., Kong, Y., Xue, N., et al., *J. Phys. Chem. C*, 2007, vol. 111, pp. 14394–14399.

23. Yu, D., Qian, J., Xue, N., Zhang, D., et al., *Langmuir*,2007, vol. 23, pp. 382–386.

24. Chen, C.Y., Xiao, S.Q., and Davis, M.E., *Microporous Mater*., 1995, vol. 4, pp. 1–20.

25. Zhao, D., Wan, Y., and Zhou, W., *Ordered Mesoporous Materials*, Weinheim: Wiley, 2013.

26. Meynen, V., Cool, P., and Vansant, E.F., *MicroporousMesoporous Mater*., 2009, vol. 125, pp. 170–223.

27. Sun, H., Han, J., Ding, Y., Li, W., et al., *Appl. Catal.,A*, 2010, vol. 390, pp. 26–34.

28. Rathousky, J., Zukal, A., Franke, O., and Schulz-Ekloff,G., *J. Chem. Soc., Faraday Trans*., 1994, vol. 90,pp. 2821–2826.

29. Schmidt, R., Stocker, M., Hansen, E.W., Akporiaye, D., et al., *Microporous Mater*., 1995, vol. 3, pp. 443–448.

30. Gerbaldi, C., Meligrana, G., Bodoardo, S., and Tuel, A.,*J. Power Sources*, 2007, vol. 174, pp. 501–507.

31. Du, Y., Yang, Y., Liu, S., Xiao, N., et al., *Microporous Mesoporous Mater*., 2008, vol. 114, 250–256.

32. Michot, L.J., Mathieu, C., and Bouquet, E.C.R., *C.R. Seances Acad. Sci., Ser. C*, 1998, vol. 1, pp. 167–174.

Tables and Figures

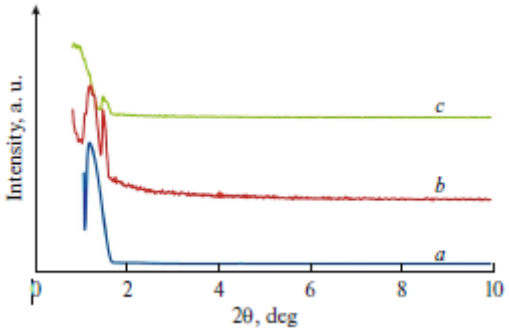

Fig. 1. XRD patterns of (*a*) SDS-B; (*b*) SDS-E and (*c*) SDS-B-450 samples

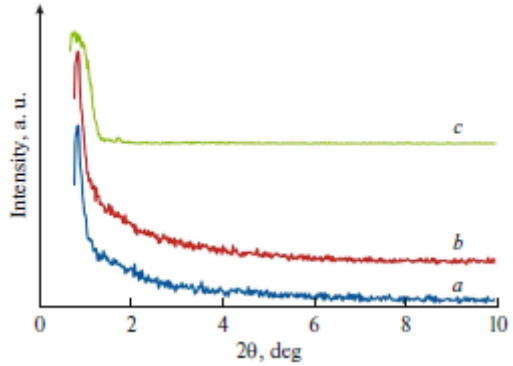

Fig. 2. XRD patterns of (*a*) CTAB-B; (*b*) CTAB-E and (*c*) CTAB-B-450 samples

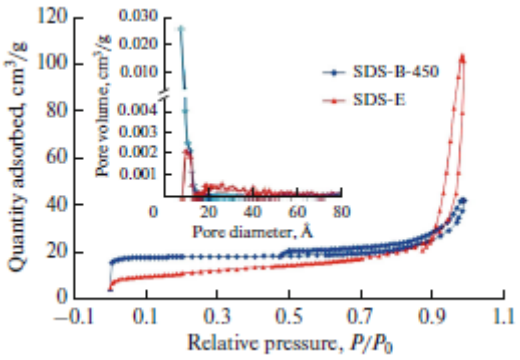

Fig. 3. Nitrogen adsorption–desorption isotherms of SDS-E and SDS-B-450 samples, the corresponding pore size distribution is shown in the inset.

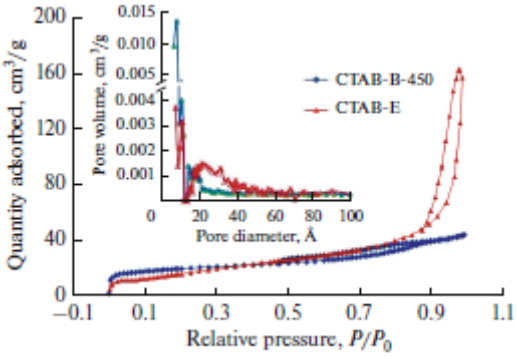

Fig. 4. Nitrogen adsorption–desorption isotherms of CTAB-E and CTAB-B-450 samples, the corresponding
pore size distribution is shown in the inset.

Table 1. Physical characteristics deducted from the treatment of nitrogen adsorption–desorption isotherms

Sample	Specific surface area, $m^2 g^{-1a}$	Total volume, $cm^3 g^{-1b}$	Pore size of the mesopores, nm[c]
SDS-E	37.3	0.156	2.54
SDS-B-450	57.1	0.064	1.01
CTAB-E	66.6	0.243	2.14
CTAB-B-450	72.4	0.070	1.45

[a]S_{BET}: specific surface area calculated by BET; [b] $V_{t,BET}$: total volume calculated by BET; [c]W: pore size of the mesopores.

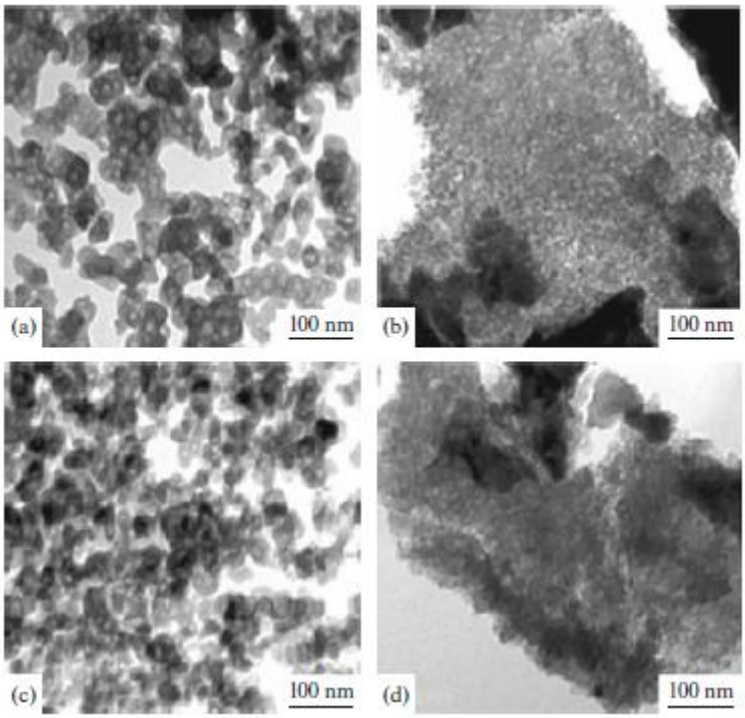

Fig. 5. TEM images of (a) SDS-E; (b) SDS-B-450; (c) CTAB-E and (d) CTAB-B-450.

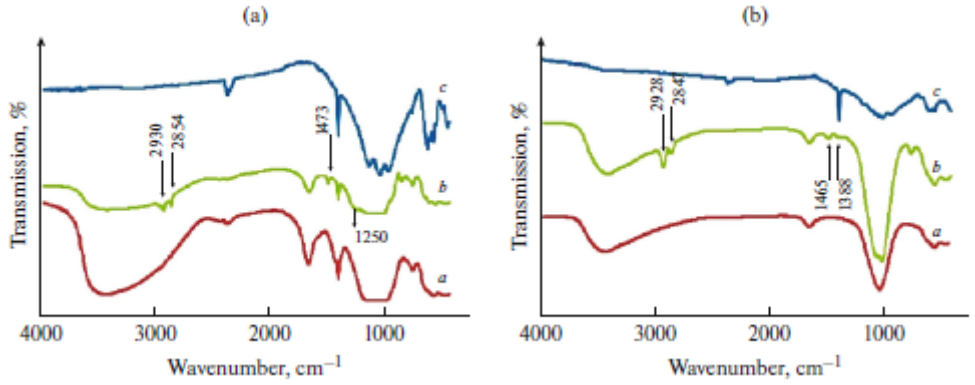

Fig. 6. FTIR spectra of samples prepared using (a) SDS ((*a*) SDS-E; (*b*) SDS-B and (*c*) SDS-B-450) and (*b*) CTAB as surfactant ((*a*) CTAB-E; (*b*) CTAB-B and (*c*) CTAB-B-450).

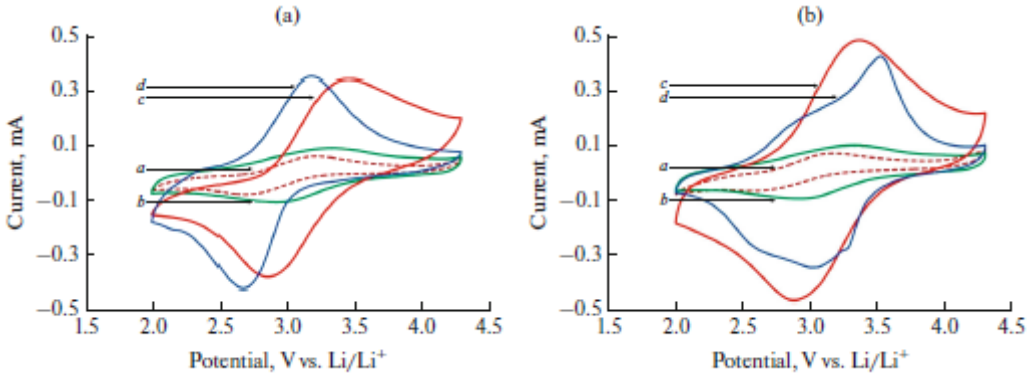

Fig. 7. Voltammograms of positive electrode containing samples prepared using (a) SDS ((*a*) SDS-B; (*b*) SDS-E; (*c*) SDS-B-450 and (*d*) SDS-B-600) and (b) CTAB as surfactant ((*a*) CTAB-B; (*b*) CTAB-E; (c) CTAB-B-450 and (*d*) CTAB-B-600) tested between 2 and 4.5 V vs. Li/Li+ at scan rate of 5 mV s^{-1}.

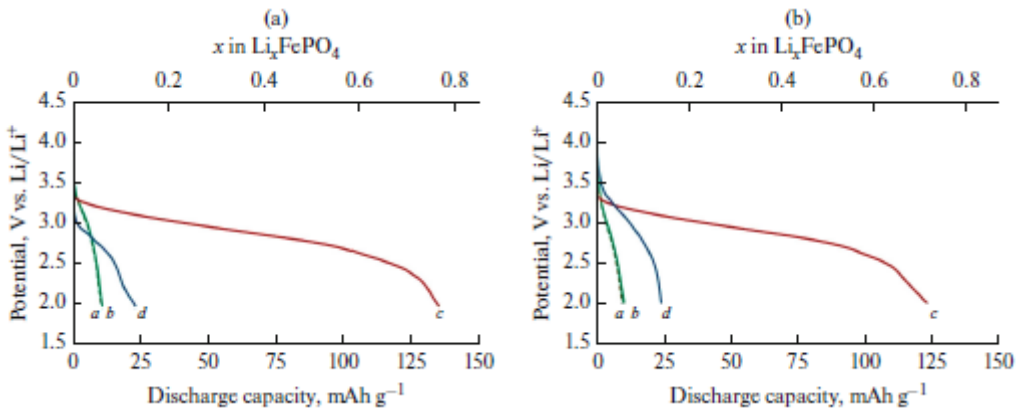

Fig. 8. Discharge curves obtained for lithium batteries with positive electrode based on samples prepared using (a) SDS ((*a*) SDS-B; (*b*) SDS-E; (*c*) SDS-B-450 and (*d*) SDS-B-600)

and (b) CTAB as surfactant ((*a*) CTAB-B; (*b*) CTAB-E; (*c*) CTAB-B-450 and (*d*) CTAB-B-600) cycled between 2.0 and 4.5 V vs. Li/Li+ at C/20 regime.

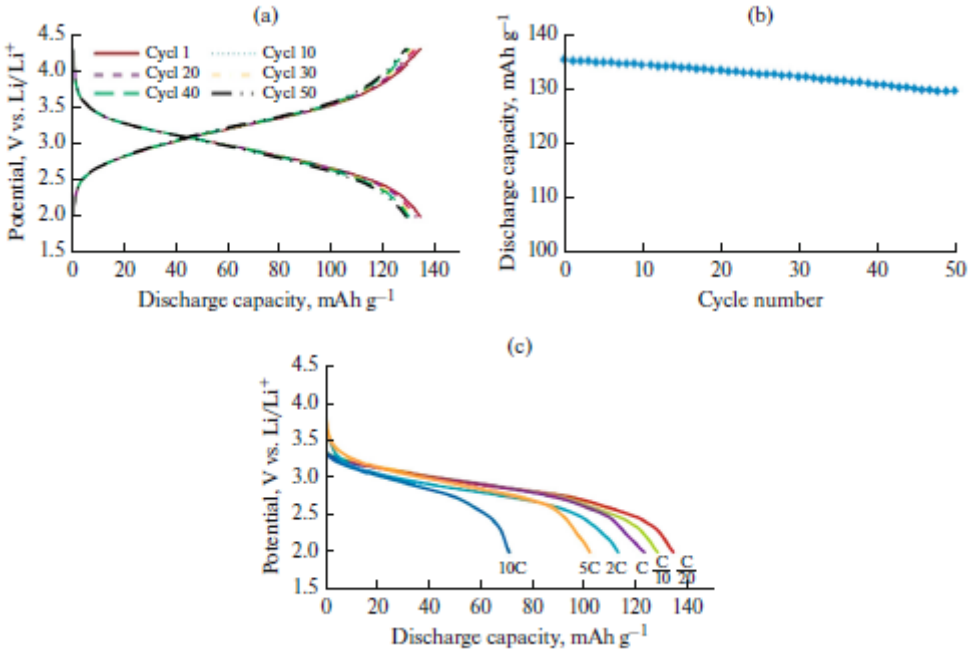

Fig. 9. (a) Selected galvanostatic discharge/charge cycles in the voltage from 2 to 4.5 V vs. Li/Li+ at C/20 regime, (b) cycling performances, and (c) rate capability of SDS-B-450 sample